International Journal of Modern Physics E

RELATIVISTIC MEAN FIELD STUDY OF ISLANDS OF INVERSION IN NEUTRON RICH Z = 17 - 23, 37 - 40 AND 60 - 64 NUCLEI

S. K. SINGH

Institute of Physics, Sachivalaya Marg, Bhubaneswar-751 005, India. *

S. MAHAPATRO

Department of Physics, Spintronic Technology and Advanced Research, Bhubaneswar-752 050, India. †

R. N. MISHRA

Department of Physics, Ravenshaw University, Cuttack, india.

We study the extremely neutron-rich nuclei for $Z = 17-23$, $37-40$ and $60-64$ regions of the periodic table by using axially deformed relativistic mean field formalism with NL3* parametrization. Based on the analysis of binding energy, two neutron separation energy, quadrupole deformation and root mean square radii, we emphasized the speciality of these considered regions which are recently predicted *islands of inversion*.

1. Introduction

The main aim of theoretical models is to explain the available experimental results and predict the properties of the atomic nuclei through out the periodic table. A good description of the properties of known nuclei gives us more confidence in extrapolating to the yet unexplored areas of the nuclear chart. The two-neutron separation energy S_{2n} systematically derived from the ground state binding energy (BE), reveal a new feature for the existence of *islands of inversion* in the exotic neutron-rich regions of nuclear landscape. The Shell Model (SM) calculation [1,2,3] is successful in nuclear structure theory. Although the application of this model in various regions explain the data quite well, it fails to reproduce the binding energy for some of the neutron-rich Ne, Na and Mg nuclei [1]. Almost two decades ago Patra et al. [4] performed the relativistic mean field (RMF) calculation with NL1 parameter set and could explain the reason of failure of shell model for these nuclei.

*Mr. S. K. Singh, Email: shailesh@iopb.res.in
†Ms. S. Mahapatro, Email: narayan@iopb.res.in

One of their explanation is the large deformation of these nuclei which are not taken in the SM calculation. Recently apart from supporting the presently known islands around ^{31}Na [5] and ^{62}Ti [6,7] regions, the INM Model [8] predict one more region around Z = 60 of stability. It was suggested that these nuclei of Z = 17 - 23, N = 38 - 42, Z= 37 - 40, N = 70 - 74 and Z = 60 - 64, N = 110 - 116 regions are deformed and form *islands of inversion* with more binding energy than their neighbouring family of isotopes. This prediction motivate us to study the properties of such nuclei and to investigate the possible reasons of the extra stability. In the present paper, we have done the calculation for these three regions by using the axially deformed RMF model.

2. Theoretical Framework

The relativistic mean field (RMF) model [9,10,11,12,13,14,15,16] become famous in recent years and have been applied to finite nuclei and infinite nuclear matter. We have taken the RMF Lagrangian [17] with NL3* parameter set [18] in our study. This force parameter is successful in both β-stable and drip-line nuclei. The Lagrangian contained the term of interaction between meson and nucleon and also self-interaction of isoscalar-scalar *sigma* meson. The other mesons are isoscalar-vector *omega* and isovector vector *rho* mesons. The photon field A_μ is included to take care of coulombic interaction of protons. A definite set of coupled equations are obtained from the above Lagrangian are solved self-consistently in an axially deformed harmonic oscillator basis. We start with the relativistic Lagrangian density for a nucleon-meson many-body system,

$$\begin{aligned}\mathcal{L} = \overline{\psi_i}\{i\gamma^\mu\partial_\mu - M\}\psi_i + \frac{1}{2}\partial^\mu\sigma\partial_\mu\sigma - \frac{1}{2}m_\sigma^2\sigma^2 \\ -\frac{1}{3}g_2\sigma^3 - \frac{1}{4}g_3\sigma^4 - g_s\overline{\psi_i}\psi_i\sigma - \frac{1}{4}\Omega^{\mu\nu}\Omega_{\mu\nu} \\ +\frac{1}{2}m_w^2V^\mu V_\mu + \frac{1}{4}c_3(V_\mu V^\mu)^2 - g_w\overline{\psi}_i\gamma^\mu\psi_iV_\mu \\ -\frac{1}{4}\vec{B}^{\mu\nu}.\vec{B}_{\mu\nu} + \frac{1}{2}m_\rho^2\vec{R}^\mu.\vec{R}_\mu - g_\rho\overline{\psi}_i\gamma^\mu\vec{\tau}\psi_i.\vec{R^\mu} \\ -\frac{1}{4}F^{\mu\nu}F_{\mu\nu} - e\overline{\psi}_i\gamma^\mu\frac{(1-\tau_{3i})}{2}\psi_iA_\mu. \qquad (1)\end{aligned}$$

Here sigma meson field is denoted by σ, omega meson field by V_μ and rho meson field is denoted by ρ_μ. A^μ denotes the electromagnetic field, which couples to the protons. ψ are the Dirac spinors for the nucleons, whose third components of isospin is τ_3 and g_s, g_2, g_3, g_ω,c_3, g_ρ are the coupling constants. The center of mass (c.m.) motion energy correction is estimated by the harmonic oscillator formula $E_{c.m.} = \frac{3}{4}(41A^{-1/3})$, where A is the mass number of the nucleus. The total quadrupole deformation parameter β_2 of the nucleus, can be obtained from the relation $Q = Q_n + Q_p = \sqrt{\frac{16\pi}{5}}(\frac{3}{4\pi}AR^2\beta_2)$, where Q_n and Q_p are the quadrupole moment for neutron and proton respectively and R is the nuclear radius. The root mean square

charge radius(r_{ch}), proton radius (r_p), neutron radius (r_n) and matter radius (r_m) are given as [19]:

$$< r_p^2 >= \frac{1}{Z} \int \rho_p(r_\perp, z) r_p^2 d\tau_p, \tag{2}$$

$$< r_n^2 >= \frac{1}{N} \int \rho_n(r_\perp, z) r_n^2 d\tau_n, \tag{3}$$

$$r_{ch} = \sqrt{r_p^2 + 0.64}, \tag{4}$$

$$< r_m^2 >= \frac{1}{A} \int \rho(r_\perp, z) r^2 d\tau, \tag{5}$$

here all terms have own usual meaning. The total binding energy and other observables are also obtained by using the standard relations, given in [17,19].

2.1. *Pairing Correlation*

Pairing correlation is playing very crucial role in open shell nuclei. In our calculation we are using the Bardeen-Cooper-Schrieffer (BCS) pairing for determining the bulk properties like binding energy (BE), quadrupole deformation parameter and nuclear radii. The pairing energy can be given as:

$$E_{pair} = -G \left[\sum_{i>0} u_i v_i \right]^2, \tag{6}$$

where G is pairing force constant and v_i^2, $u_i^2 = 1 - v_i^2$ are occupation probabilities respectively [20,21,22]. The simple form of BCS equation can be derived from the variational method with respect to the occupation number v_i^2:

$$2\epsilon_i u_i v_i - \triangle(u_i^2 - v_i^2) = 0, \tag{7}$$

using $\triangle = G \sum_{i>0} u_i v_i$. The above equation 7 is known as BCS equation for pairing energy.

The occupation number is defined as:

$$n_i = v_i^2 = \frac{1}{2} \left[1 - \frac{\epsilon_i - \lambda}{\sqrt{(\epsilon_i - \lambda)^2 + \triangle^2}} \right]. \tag{8}$$

In our calculation we are dealing with the nuclei far away from beta stability line, so the constant gap for proton and neutron used here is valid in considered region. These constant gap equation for proton and neutron is taken from Ref. [23,24] which is given as:

$$\triangle_p = R B_s e^{sI - tI^2} / Z^{1/3} \tag{9}$$

and

$$\triangle_n = R B_s e^{-sI - tI^2} / A^{1/3}, \tag{10}$$

with R=5.72, s=0.118, t= 8.12, B_s=1, and $I = (N - Z)/(N + Z)$.

In our present calculation, we have taken the constant pairing gap for all states $\mid \alpha >= \mid nljm >$ near the Fermi surface for the shake of simplicity. As we know, if we go near the very neutron drip line, then coupling to the continuum become important [25,26]. In this case we should use the Relativistic Hartree-Bogoliubov (RHB) approach which is more accurate formalism for this region. But by using BCS pairing correlation model, it has been shown that the results from relativistic mean field BCS (RMF-BCS) approach is almost similar with the RHB formalism [27,28,29,30,31].

2.2. *Choosing the Basis*

We divide our calculation between three regions: first region having Z=17 -23, and second region Z= 37-40 and third region Z=60 - 64. For checking the proper basis, we calculate the physical observables like binding energy, root mean square (rms) radii and quadrupole deformation parameter(β_2). So we have taken heavier nuclei from each region for example ^{69}V from region I, ^{119}Zr from region II and ^{185}Gd from region III. We have presented our calculations in table 2.2, with N_F=N_B =6 to 16, in the interval of 2, at the initial deformation of β_2=0.2, using the NL3* parameter set. For ^{69}V nuclei; BE, rms radii and β_2 are almost same for N_F=N_B $\geq$ 10. It means, we can take N_{max} = 10 for boson and Fermion harmonic basis for region I. In ^{119}Zr nucleus; these physical observables change from N_F=N_B= 10 to 12. but become constant after N_F=N_B= 12. Then if we combine these two region and take N_{max}=12, then we have enough space for both region. One can easily see that for ^{185}Gd nucleus N_{max}=12 is not sufficient model space. It needs more space for calculation. Therefore, in this paper, we have taken N_{max}=12 for region I, II and N_{max}=14 for region III. Similar calculation are found in Ref. [32].

The physical observables like binding energy, root mean square(rms) radii and quadrupole deformation parameter(β_2) does not much change when blocking is applied [27]. We have given our calculated results in table 2.2. The RMF values of the observables without blocking remains same with the values of blocking. If we see the table 2.2, the difference between blocking and without blocking is nearly less than 1 MeV.

3. Choosing Reference Frame

While comparing our binding energy results with macro-microscopic (MM) approach, some important points needed to be stated. It is a known feature in MM models that the order of accuracy varies from region to region [8] in the N-Z plane. The degree of disagreement is unacceptably large even slightly away from the known

Table 1. Calculated binding energy BE(MeV), root mean square r_{ch}, r_n, r_p, r_m and quadrupole deformation parameter β_2 at different bosonic and Fermionic basis harmonic quanta. Root mean square radius are in fm. During this calculation we have taken initial deformation parameter β_0 equal to 0.2.

Nucleus	Basis	BE	r_{ch}	r_n	r_p	r_m	β_2
^{69}V	6	508.810	3.733	4.103	3.646	3.956	0.160
	8	525.829	3.822	4.236	3.738	4.077	0.220
	10	530.960	3.827	4.301	3.742	4.123	0.237
	12	531.547	3.831	4.330	3.747	4.145	0.247
	14	531.651	3.832	4.343	3.747	4.154	0.249
	16	531.779	3.831	4.355	3.747	4.162	0.251
^{119}Zr	6	816.970	4.302	4.810	4.227	4.622	0.139
	8	904.886	4.500	4.903	4.428	4.749	0.084
	10	919.504	4.518	4.986	4.447	4.811	0.055
	12	922.347	4.525	5.018	4.454	4.836	0.011
	14	922.768	4.525	5.025	4.454	4.841	0.006
	16	922.868	4.524	5.031	4.453	4.844	0.005
^{185}Gd	6	1057.418	4.783	5.507	4.716	5.247	0.139
	8	1341.916	5.155	5.520	5.092	5.376	0.106
	10	1395.818	5.280	5.661	5.219	5.512	0.118
	12	1406.994	5.294	5.721	5.233	5.557	0.122
	14	1408.427	5.289	5.737	5.228	5.566	0.114
	16	1408.222	5.289	5.741	5.228	5.569	0.114

domain (See Figs. 7-9, Ref. [8] and Fig. 1, Ref. [33]). On the other hand a microscopic formalism based on nuclear Lagrangian/Hamiltonian predicts physical observables through out the known/unknown territory of the periodic chart equally well. The parameters of these models have been determined by fitting the experimental data of few well known nuclei only. It is to be noted that the prediction of nuclei even in the known region are treated in an equal footing with the unknown region. Therefore, similar predictive power can be expected in the actual unknown region.

4. Calculations and Results

Relativistic mean field model have given very good result in β stable nuclei of the nuclear landscape. In this work we are analyzing the exotic neutron drip line nuclei by using RMF model with recent well known NL3* [18] parameter set. We obtain matter radii, quadrupole deformation parameter and ground state binding energies of these exotic nuclei of Z = 17-23, 37-40 and Z = 60-64 regions. The calculated results, like binding energy, radii, quadrupole deformation are given in tables (3-5) and the results are discussed in figures 1-10. In upcoming subsections we have described these results in detail.

Table 2. Calculated ground state binding energy BE(MeV), root mean square r_{ch}, r_n, r_p, r_m and quadrupole deformation parameter β_2 without blocking and with blocking. Root mean square radius are in fm.

Nucleus	Without Blocking						With Blocking					
	BE	r_{ch}	r_n	r_p	r_m	β_2	BE	r_{ch}	r_n	r_p	r_m	β_2
^{51}Cl	385.05	3.49	4	3.39	3.81	-0.25	384.46	3.49	4	3.39	3.81	-0.25
^{63}Cl	390.19	3.63	4.51	3.54	4.27	0.31	389.97	3.63	4.51	3.54	4.27	0.31
^{51}Ar	402.94	3.5	3.94	3.41	3.76	-0.23	402.48	3.5	3.94	3.4	3.76	-0.23
^{63}Ar	416.23	3.65	4.41	3.56	4.19	0.23	416	3.65	4.4	3.56	4.18	0.22
^{53}K	423.78	3.5	3.96	3.41	3.77	0	423	3.51	3.96	3.41	3.77	-0.01
^{62}K	441.36	3.65	4.3	3.56	4.09	0.12	440.79	3.65	4.3	3.56	4.09	0.12
^{55}Ca	446.46	3.56	3.98	3.47	3.8	0	445.91	3.56	3.98	3.47	3.8	-0.03
^{65}Ca	465.8	3.7	4.34	3.61	4.13	0.14	465.55	3.7	4.34	3.61	4.13	0.14
^{56}Sc	461.32	3.6	3.97	3.51	3.8	0	460.78	3.6	3.97	3.51	3.8	0
^{66}Sc	487.47	3.74	4.33	3.66	4.12	0.18	486.79	3.74	4.32	3.66	4.12	0.18
^{57}Ti	475.64	3.64	3.96	3.55	3.81	-0.1	475.08	3.64	3.96	3.55	3.81	-0.1
^{57}V	484.57	3.68	3.91	3.59	3.79	0.17	483.79	3.68	3.91	3.59	3.79	0.17
^{68}V	529.77	3.82	4.3	3.74	4.12	0.23	528.93	3.82	4.29	3.74	4.11	0.23
^{103}Rb	832.98	4.42	4.81	4.35	4.65	-0.27	832.42	4.41	4.81	4.34	4.65	-0.26
^{110}Rb	853.43	4.43	4.94	4.35	4.75	-0.06	852.67	4.43	4.94	4.35	4.75	-0.07
^{105}Y	863.76	4.44	4.79	4.37	4.64	-0.23	863.17	4.45	4.79	4.38	4.64	-0.24
^{107}Zr	882.85	4.47	4.81	4.4	4.66	-0.23	882.4	4.48	4.81	4.4	4.66	-0.24

4.1. *Binding Energy*

Binding energy (BE) is precisely observed from experiment which is responsible for stability and structure of the nuclei. The maximum binding energy corresponds to the ground state for a given nucleus and all other solutions are intrinsic excited states. We have given RMF, FRDM [34,35], INM ground state binding energy in second, third and fourth column of the tables (tables 3 - 5) respectively. In fifth column $\triangle E_1$ which indicates the binding energy difference between FRDM and RMF i.e. BE(FRDM) - BE(RMF) and in sixth column $\triangle E_2$ indicates the binding energy difference between INM and RMF i.e. BE(INM) - BE(RMF). Last two columns for quadrupole deformation parameter (QDP)(β_2) of RMF and FRDM model respectively. In this subsection we are comparing our RMF binding energy (BE) with INM (BE) [8] and well established FRDM (BE) [35] results.

In fig. 1(a), in $Z = 17 - 23$ region, we have plotted the binding energy difference $\triangle$E for Cl isotopes. We get $\triangle E_2$ is zero means RMF and INM binding energies are nearly same at lower mass region, but if we go further, difference will increase in middle part and at A = 58, 59 again it goes to nearly zero, but diverges at higher mass region. If we compare our result with FRDM, then we got $\triangle E_1$ nearly zero at lower mass region, but it diverges at higher mass region. In Fig 1(b), in case of Ar

isotopes. The RMF BE is not consistent with INM at lower mass region but we get $\triangle E_2$ nearly zero at middle region at A = 54 - 60, which again diverges at higher mass region. If we compare our results with FRDM, then we get $\triangle E_1$ nearly zero at lower mass region at A = 51 - 56 then the difference increases at higher mass region at A = 56 - 61. In Fig 1(c), RMF binding energy is very close to INM in lower mass region at A = 52, 54 then $\triangle E_2$ increases within A = 55 − 60 in the middle region. Further it is very close to INM binding energy. If we compare our results with FRDM, then $\triangle E_1$ tends to zero at A= 53 then $\triangle E_1$ increases further. In Fig 1(d), in case of Ca, RMF binding energy is very close to INM and FRDM binding energy at lower mass region at A = 53, 56. RMF binding energy diverges from both model (INM and FRDM) in the middle part A = 56 - 62 and then matches at higher mass region. In Fig 1(e), in case of Sc, we got $\triangle E_1$ and $\triangle E_2$ are zero in lower mass, whereas both diverge in the middle part A = 53 - 63 then it further moves to zero. In the Fig 1(f), $\triangle E_1$ and $\triangle E_2$ are following the same trend as Fig 1(e) but it diverges in A = 58 - 62, and at higher region RMF BE matches with FRDM and INM predictions.

The binding energy difference for Rb isotopes is given in Fig. 2(a), the $\triangle E_1$ has a large value at lower mass A = 103 - 107, then it tends to zero in higher region but if we compare RMF with INM results, $\triangle E_2$ increases in lower mass region and go to zero in middle region then diverges at higher mass A = 107 - 114 region. In Fig. 2(b), we plotted the $\triangle E_1$ and $\triangle E_2$ for Sr isotopes. We got same trend but RMF results diverges from INM at higher mass region while it closes to FRDM. In lower mass region RMF results are not matching with INM and FRDM results. Energy difference $\triangle$E for Y nuclei isotopes are given in Fig. 2(c), again RMF results are not consistent with INM and FRDM results at lower mass A = 105 - 108, but at higher mass region it matches with INM and FRDM results. Fig. 2(d), represent $\triangle E_1$ and $\triangle E_2$ for Zr isotopes, from figure it is clear that our RMF results are not matching with INM and FRDM results.

In Fig. 3, we have given $\triangle$E (binding energy difference) for region Z = 60 - 64 nuclei. For Nd isotopes, RMF binding energy is not consistent with FRDM at A = 166 -180. Later on RMF binding energy is close to FRDM result for few isotopes A = 179 - 181 then again diverges at A = 182. When we compare our result with INM binding energy, the binding energy of RMF is very close to it at A = 168 - 170 and later on diverges with increase in mass number. In case of Pm nuclei isotopes, which is plotted in Fig. 3(b), RMF result is not consistent with FRDM for the whole region. If we compare our result with INM region, it is consistent till A = 168 - 172 and then diverges. In Sm isotopes, RMF binding energy is not consistent with FRDM in whole region. $\triangle E$ for Sm has followed the same trend as $\triangle E$ of Pm nuclei isotopes i.e. matches at lower mass region and diverge at higher mass region for both FRDM and INM results. In Eu nuclei isotopes, RMF BE does not consistent with FRDM and INM binding energy, in both case $\triangle$E increases with mass numbers.

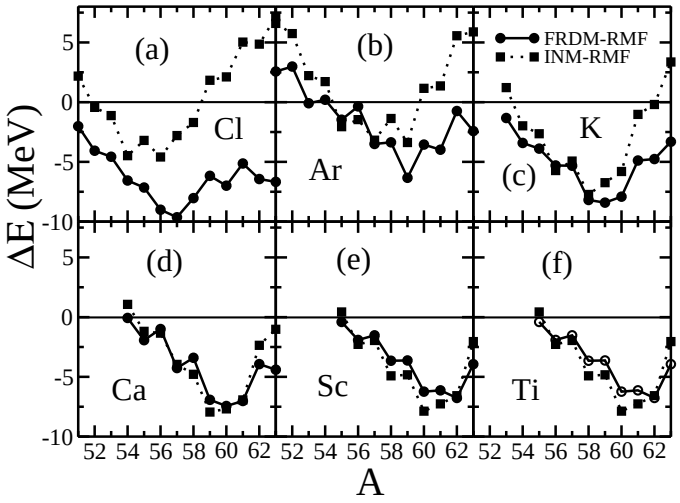

Fig. 1. Difference between the binding energies using RMF, Finite Range Droplet Model (FRDM), Infinite Nuclear Matter (INM) model (a) The circle represent for $\triangle E_1$(FRDM - RMF) (b) The square represent for $\triangle E_2$ (INM - RMF) model for different mass values of Z = 17 - 23 region.

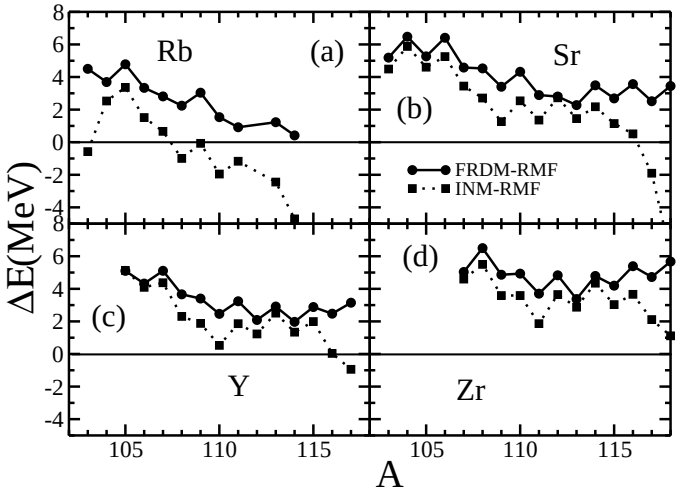

Fig. 2. Same as Fig. 1 for Z = 37 - 40 region.

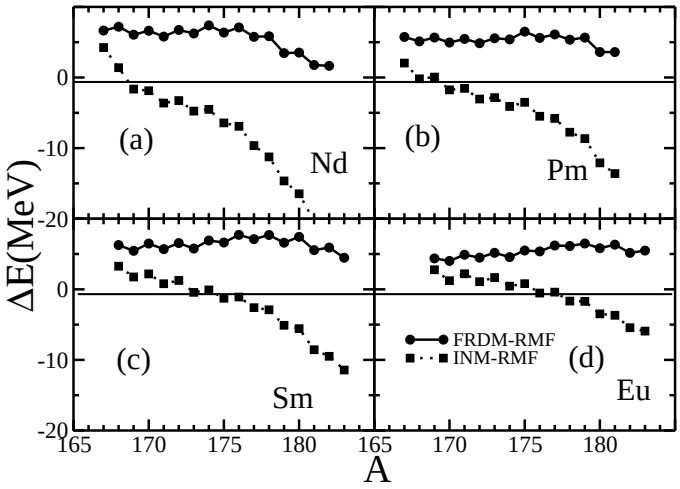

Fig. 3. Same as Fig. 1 for Z = 60 - 64 region.

4.2. *Quadrupole Deformation*

Quadrupole deformation parameter (QDP) β_2 is directly connected to the shape of the nucleus. It is very common to say that if we go towards drip-line nuclei, deformation will gradually increase but recently experimental paper of Tshoo [36] explain that ^{22}O is prolate in shape but ^{24}O is spherical in structure. Keeping this result in our mind we have calculated the QDP β_2 for recently predicted *island of inversion* region in nuclear landscape. Because of the unavailability of experimental data of these nuclei, we have compared our calculated QDP β_2 with well stabilized FRDM [34]data. In Fig. 4, we have plotted the quadrupole deformation parameter β_2 for RMF and FRDM models as a function of mass number for Z = 17 - 23 region. In Cl case, QDP β_2 continuously increases with the mass number, as shown in Fig. 4(a). In lower mass region Cl isotopes are oblate and in higher mass region these are prolate and middle case A = 56 - 58, there is continuous shape change from oblate to prolate. If we compare RMF results with FRDM predictions then we get totally different result in FRDM. In FRDM, shape is suddenly changed from oblate to prolate (A = 54) and prolate to oblate (A = 57). Most of the Cl isotopes are oblate in FRDM model. There are continuous changes in deformation but there is very small amount of energy difference (1 MeV) between ground state and first excited state. So we can say that other shape is also possible, But here we are taking only the ground state and neglecting the other possibility of shapes. In Ar case, most of the isotopes are oblate in lower mass region A = 52 - 57, and some are spherical at A = 59 - 60 then in higher region it again changes its shape from oblate to prolate in RMF model. When we compare with FRDM data, RMF is very close to FRDM except middle and high region in Fig. 4(b). FRDM is completely oblate

in shape over the region. In Fig. 4(c), we have plotted the QDP β_2 for K isotopes. From figure it is very clear that most of the isotopes are spherical in shape. When we compare with FRDM data, it shows the same trend as RMF at A = 54-57 i.e. spherical in shape. In Ca, Sc, Ti case all are spherical in shape over all isotopes.

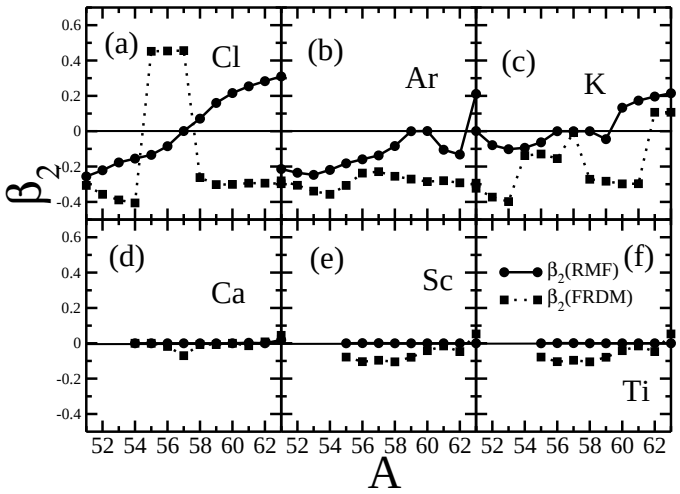

Fig. 4. Quadrupole Deformation Parameter obtained from RMF(NL3*) (circle) compared with the FRDM(square) results for different isotopes of Z = 17 - 23 region.

Deformation parameter for Rb isotopes are given in fig. 5(a). From the figure it is clear that most of the isotopes are spherical shape but in lower mass region A = 103 - 105, it is oblate. If we see the QDP β_2 for Rb isotopes in FRDM model, we found that most are in prolate shape in lower mass region A = 103 - 110 then shape changes to oblate which is totally different from RMF result. Sr isotopes are given in fig. 5(b), for Sr isotopes, most of the nuclei are in spherical but in lower mass A = 104 - 106 are prolate and at A = 103 shape changes from prolate to oblate. If we see the result of FRDM, most of the Sr isotopes are prolate and in higher region it is spherical. RMF matches to FRDM at A = 104 - 106 and in higher region. Again we are getting spherical shape for A = 108 - 117 for Y isotopes in fig. 5(c). RMF matches only at A = 106, 107 and in higher mass A = 114 - 116. In Zr isotopes, It is spherical in shape at A = 109- 120 except A = 114, 115 as shown in the fig. 5(d). If we go from A = 107 to 109, then we got a sharp shape change at A = 108 i.e. oblate to prolate and again prolate to spherical. FRDM have prolate shape in lower mass region A = 107 - 113 and then changes to oblate in A = 114 - 120.

In Fig. 6(a), for Nd isotopes, at A = 167 -174, both RMF and FRDM are prolate in shape but when we go further RMF change its shape to oblate in A = 175 - 179 region while FRDM remains prolate in shape. In higher mass region A = 180 -

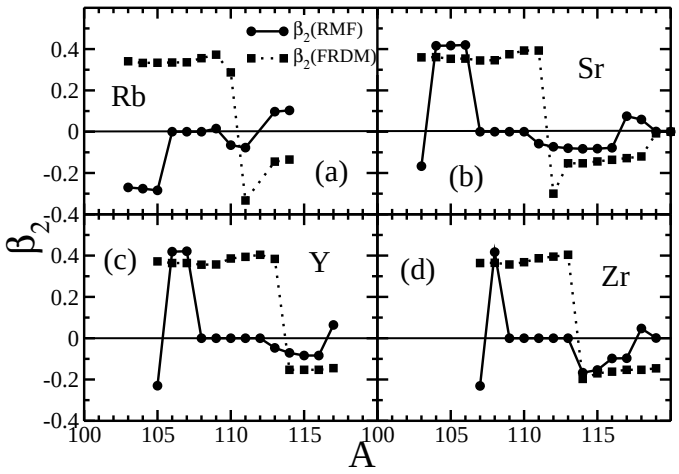

Fig. 5. Same as Fig. 4 for Z = 37 - 40 region.

182 RMF goes oblate to nearly spherical and FRDM goes from prolate to oblate it means these two model are not consistent in A = 175 - 182. Isotopes of Pm are given in fig. 6(b). Here we get consistent result in RMF and FRDM model at A = 167 - 175. Then RMF changes to oblate in higher mass region and again change to nearly spherical while FRDM does not change the shape. In Sm case, both models match to each other in A = 168 - 176 then RMF goes to oblate and spherical shape where FRDM does not follow the RMF trend except A = 181, 182. In Eu isotopes as shown in fig.6(d), both RMF and FRDM show consistency at A = 169-178, later on RMF changes to oblate at A= 179-182. FRDM is matching with RMF at A =181,182 only at higher mass region.

4.3. *Nuclear Radius*

In this subsection we are concentrating on the neutron radius (r_n), proton radius (r_p), charge radius (r_{ch}) and matter radius (r_m) which are calculated by using RMF(NL3*) formalism. In Fig. 7, we have plotted the r_n, r_p, r_{ch}, and r_m for Cl, Ar, K, Ca, Sc, Ti and V nuclei. In Z = 17 - 23 region, all the radii increase monotonically with mass number. In Fig. 8, we have plotted the r_n, r_p, r_{ch}, r_m with mass number for Z = 37-40 region. In Rb isotopes, there is a sharp fall in radii till A=106, then radii increase monotonically. In Sr isotopes, the radii follow same trend as Rb isotopes but in this case fall at A=107, then the radii increase monotonically. In Y isotopes, the radii follow a jump at A=106 and remain constant upto A = 107, then decrease at A=108. Later on the radii follow the same trend means the radii increase monotonically with mass number. In Zr isotopes, the radii increase and it follow a jerk at A = 108 then go down at A = 109 and later on

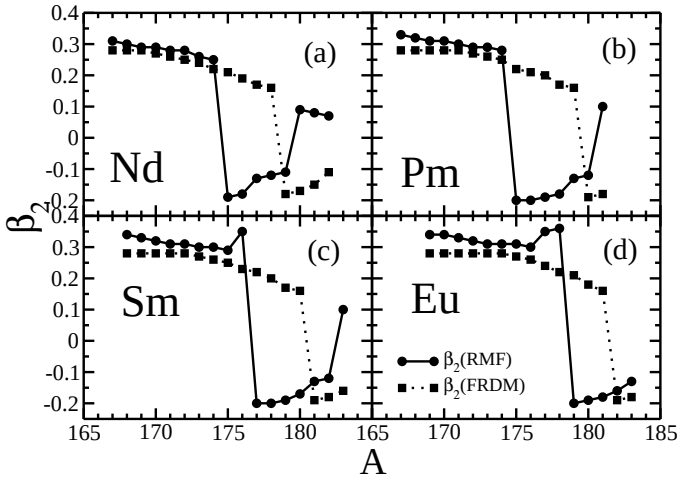

Fig. 6. Same as Fig. 4 for Z = 60 - 64 region.

increase. In Fig. 9, we have plotted the radius curve for Z = 60 - 64 region, in the case of Nd, Pm isotopes the radii increase monotonically with atomic number. In Sm (Fig. 9c) isotopes, we get a small jerk in A = 176 while in Eu (Fig. 9d) isotopes this jerk arises at A = 177-178, then increases monotonically saying a change in the deformation of the nuclei.

4.4. *Two-neutron separation energy*

The two-neutron separation energy S_{2n}(N,Z) = BE(N, Z) - BE(N-2, Z) is shown in Fig. 10. The S_{2n} values decrease gradually with increase in neutron number. It is indeed satisfying to note that in the recent years strong evidences both experimental and theoretical have emerged [6,7] supporting the existence of this island of inversion centering around ^{62}Ti. We can predict the stability of these nuclei by S_{2n} energy. If S_{2n} is large, it means nuclei will be stable with two-neutron separation. As shown in first part (a) of Fig. 10, in Z = 17-23 region, we are getting a sharp down curve for all the members of this region at N = 42. So we can say that this may be the neutron magic number in this neutron-dripline nuclei. In S_{2n} plot for Ti, we are getting a small considerable jerk at N = 44. This shows the extra stability of nuclei. In Sc, S_{2n} plot follow the same trend as in Ti, but the magnitude is very small. In other cases, i.e. Z = 17, 18, 19, 20 region, there is no any local extra stability. In second part (b), we are getting a sharp down curve at N = 68 for all the members of this region. In Sr, Rb, there is a small jerk at N = 74. In other cases, there is no local stability. In third part (c), for Z = 60 - 64 region, there is a sharp fall at N = 112 for all the members of this region. We get local extra stability in Nd, Pm and other nuclei also follow nearly the same trend.

Table 3. We have given ground state binding energy (BE) for RMF(NL3*), FRDM, INM and comparison between calculated BE using RMF(NL3*)model with FRDM($\triangle E_1$) and INM ($\triangle E_2$) and β_2 for Z = 17 - 23 region. Binding energies are in MeV.

nucleus	BE(RMF)	BE(FRDM)	BE(INM)	$\triangle E_1$	$\triangle E_2$	β_2(RMF)	β_2(FRDM)
^{51}Cl	385.1	383.1	387.2	-2.02	2.18	-0.256	-0.307
^{52}Cl	386.9	382.9	386.5	-4.07	-0.44	-0.221	-0.357
^{53}Cl	388.8	384.3	387.7	-4.57	-1.13	-0.177	-0.389
^{54}Cl	390.4	383.8	385.9	-6.56	-4.48	-0.155	-0.406
^{55}Cl	391.9	384.7	388.7	-7.15	-3.20	-0.134	0.452
^{56}Cl	393.0	384.0	388.5	-9.01	-4.59	-0.085	0.454
^{57}Cl	394.7	385.1	391.9	-9.64	-2.80	0.001	0.456
^{58}Cl	393.5	385.4	391.8	-8.04	-1.70	0.071	-0.262
^{59}Cl	392.7	386.6	394.6	-6.17	1.83	0.160	-0.302
^{60}Cl	392.2	385.2	394.3	-6.99	2.12	0.216	-0.301
^{61}Cl	391.8	386.6	396.8	-5.14	5.03	0.254	-0.294
^{62}Cl	390.9	384.5	395.8	-6.44	4.86	0.283	-0.294
^{63}Cl	390.2	383.5	397.4	-6.67	7.17	0.310	-0.297
^{49}Ar	395.9	396.3	399.9	0.44	4.01	-0.201	-0.223
^{50}Ar	399.5	401.0	405.3	1.49	5.84	-0.217	-0.248
^{51}Ar	399.5	402.0	406.1	2.57	6.59	-0.214	-0.281
^{52}Ar	402.9	405.9	408.7	2.98	5.74	-0.235	-0.306
^{53}Ar	406.2	406.1	408.5	-0.09	2.22	-0.247	-0.339
^{54}Ar	408.7	408.9	410.4	0.2	1.72	-0.219	-0.357
^{55}Ar	411.1	409.6	409.0	-1.47	-2.05	-0.182	-0.307
^{56}Ar	413.3	412.9	411.8	-0.36	-1.46	-0.159	-0.237
^{57}Ar	415.4	411.9	412.2	-3.5	-3.18	-0.137	-0.229
^{58}Ar	416.9	413.6	415.6	-3.36	-1.37	-0.084	-0.255
^{59}Ar	419.1	412.8	415.8	-6.33	-3.38	0.000	-0.271
^{60}Ar	418.2	414.6	419.3	-3.55	1.16	0.001	-0.285
^{61}Ar	417.9	413.9	419.2	-3.98	1.36	-0.105	-0.280
^{62}Ar	416.8	416.0	422.3	-0.74	5.56	-0.132	-0.292
^{63}Ar	416.3	413.8	422.1	-2.42	5.89	0.211	-0.294
^{53}K	423.8	422.5	425.0	-1.33	1.22	0.001	-0.323
^{54}K	427.1	423.7	425.1	-3.41	-1.98	-0.079	-0.373
^{55}K	430.4	426.5	427.8	-3.89	-2.64	-0.102	-0.398
^{56}K	433.5	428.2	427.8	-5.30	-5.72	-0.094	-0.138
^{57}K	436.4	431.1	431.5	-5.32	-4.93	-0.063	-0.129
^{58}K	439.5	431.4	431.8	-8.19	-7.73	0.000	-0.155
^{59}K	442.8	434.3	436.0	-8.41	-6.74	0.000	-0.008
^{60}K	442.4	434.5	436.6	-7.91	-5.80	0.000	-0.272
^{61}K	441.6	436.7	440.6	-4.88	-1.03	-0.045	-0.283
^{62}K	441.4	436.6	441.2	-4.76	-0.20	0.133	-0.298
^{63}K	441.4	438.0	444.7	-3.31	3.37	0.173	-0.297
^{54}Ca	442.7	442.7	443.7	-0.07	1.07	0.000	0.000
^{55}Ca	446.5	444.5	445.3	-1.93	-1.19	0.000	0.000
^{56}Ca	450.2	449.2	448.8	-1.00	-1.34	0.000	-0.018
^{57}Ca	454.0	449.7	450.0	-4.26	-3.95	0.000	-0.070
^{58}Ca	457.9	454.5	453.1	-3.40	-4.79	0.000	-0.007
^{59}Ca	461.9	455.0	453.9	-6.92	-7.95	0.000	-0.007
^{60}Ca	465.6	458.2	457.9	-7.44	-7.68	0.000	0.000
^{61}Ca	465.9	458.9	459.0	-7.02	-6.93	0.003	-0.014
^{62}Ca	465.6	461.7	463.3	-3.93	-2.36	0.000	0.008
^{63}Ca	465.3	460.9	464.3	-4.4	-1.02	0.019	0.045
^{64}Ca	465.6	463.4	468.4	-2.21	2.76	0.126	0.045
^{65}Ca	465.8	462.6	469.2	-3.21	3.39	0.154	0.071
^{66}Ca	466.0	464.6	472.6	-1.33	6.64	0.172	0.062

continued

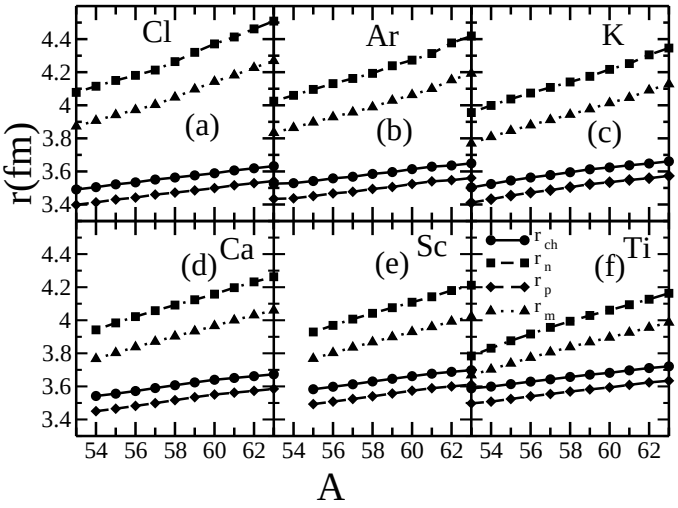

Fig. 7. The charge radii r_{ch} (circle), The neutron radius r_n (square), The proton radius r_p (diamond), the rms radii r_m of matter distribution (triangle up) for different isotopes of Z = 17 - 23 region using the RMF(NL3*) formalism.

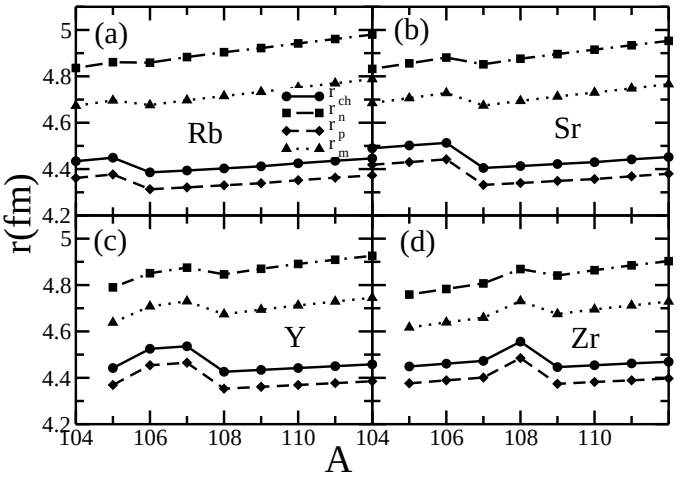

Fig. 8. Same as Fig. 7 for Z = 37 - 40 region .

5. Discussion and Remarks

Taking RMF as a reference, we evaluate $\triangle E_1$ and $\triangle E_2$. Analyzing fig. 1, we find both $\triangle E_1$ and $\triangle E_2$ similar for all the considered six nuclei, Cl to Ti. The large value

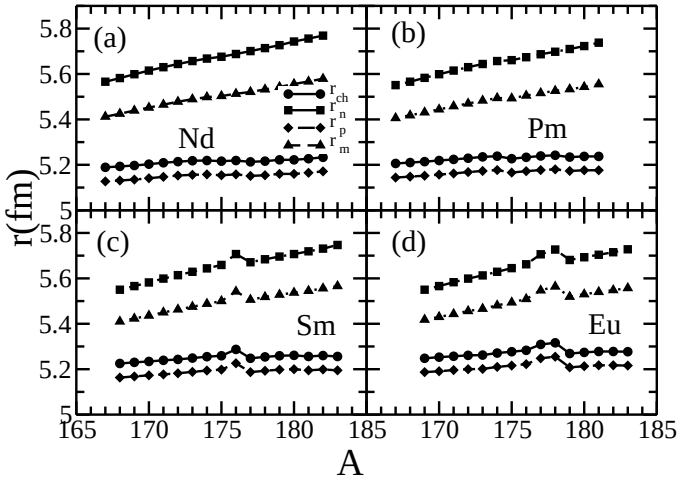

Fig. 9. Same as Fig. 7 for Z = 60 - 64 region .

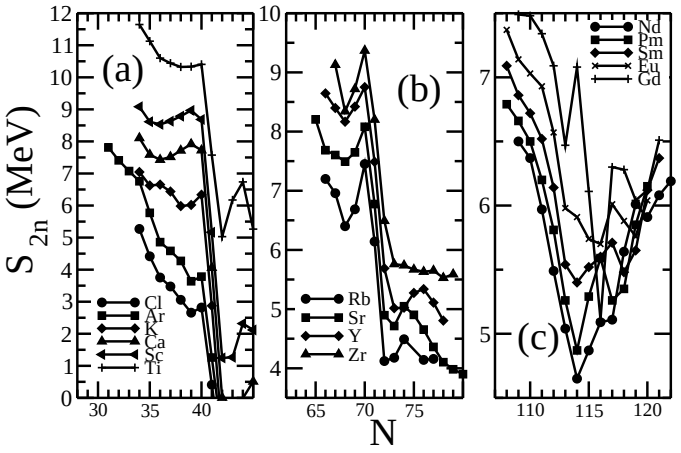

Fig. 10. The two-neutron separation energy S_{2n} for different isotopes of Z = 17 - 23, 37 - 40, 60-64 region by using RMF(NL3*) formalism.

of $\triangle E_1$ and $\triangle E_2$ at middle of the region shows the speciality of these nuclei, except Cl isotopes [fig. 1(a)]. All other isotopes show similar trend with INM and FRDM. From fig. 2 and fig. 3, $\triangle E_1$ are almost constant, if one extends the calculation to higher mass number in isotopic chain. On the other hand, calculated $\triangle E_2$ goes on increasing with A. In this situation, the predictive power of RMF, FRDM and INM are questionable. For example, (1) if we consider RMF as the absolute reference

continued

nucleus	BE(RMF)	BE(FRDM)	BE(INM)	$\triangle E_1$	$\triangle E_2$	β_2 (RMF)	β_2(FRDM)
^{55}Sc	457.1	456.7	457.5	-0.40	0.43	0.000	-0.078
^{56}Sc	461.3	459.4	459.0	-1.91	-2.28	0.001	-0.104
^{57}Sc	465.6	464.1	463.7	-1.53	-1.96	0.001	-0.096
^{58}Sc	470.0	466.3	465.0	-3.65	-4.91	0.000	-0.105
^{59}Sc	474.4	470.8	469.6	-3.62	-4.83	0.000	-0.079
^{60}Sc	478.9	472.7	471.0	-6.24	-7.87	0.000	-0.042
^{61}Sc	483.1	477.0	475.8	-6.13	-7.26	0.000	-0.015
^{62}Sc	484.1	477.3	477.5	-6.77	-6.58	0.000	-0.047
^{63}Sc	484.3	480.4	482.3	-3.94	-2.05	0.000	0.053
^{64}Sc	485.4	481.2	483.6	-4.18	-1.71	0.108	0.073
^{65}Sc	486.6	483.8	488.0	-2.81	1.31	0.166	0.090
^{66}Sc	487.5	484.1	489.2	-3.35	-1.70	0.181	0.116
^{50}Ti	435.5	438.7	437.6	3.20	2.19	0.005	0.000
^{51}Ti	442.7	444.8	444.0	2.07	1.28	0.006	0.000
^{52}Ti	448.7	452.7	452.6	3.97	3.83	0.000	0.000
^{53}Ti	454.5	457.1	457.4	2.66	2.88	0.001	0.000
^{54}Ti	460.0	464.2	464.5	4.12	4.45	0.048	0.000
^{55}Ti	465.4	467.9	468.1	2.47	2.63	0.085	0.134
^{56}Ti	470.7	474.4	474.1	3.69	3.40	0.103	0.135
^{57}Ti	475.7	477.1	476.7	1.45	1.06	-0.104	0.135
^{58}Ti	480.6	483.1	482.0	2.47	1.44	-0.095	-0.105
^{59}Ti	485.3	485.5	484.1	0.122	-1.29	-0.078	-0.105
^{60}Ti	490.0	491.0	488.9	1.07	-0.98	0.001	-0.079
^{61}Ti	495.0	493.1	491.0	-1.87	-4.05	0.000	-0.018
^{62}Ti	499.7	497.9	495.9	-1.75	-3.77	0.000	0.000
^{63}Ti	501.4	498.8	498.1	-2.54	-3.30	0.000	-0.042
^{64}Ti	502.4	503.4	503.2	1.05	0.86	-0.035	0.027
^{65}Ti	505.5	503.8	504.7	-1.65	-0.80	0.167	0.062
^{57}V	484.6	486.5	486.7	1.94	2.09	0.167	0.181
^{58}V	490.0	490.5	490.1	0.45	0.13	0.150	0.163
^{59}V	495.2	496.7	496.1	1.53	0.95	-0.125	0.162
^{60}V	500.4	499.8	498.9	-0.60	-1.54	-0.107	-0.130
^{61}V	505.4	505.5	504.4	0.05	-1.07	-0.071	-0.104
^{62}V	510.8	508.6	506.8	-2.17	-3.95	0.000	-0.044
^{63}V	515.9	513.8	512.1	-2.11	-3.80	0.000	0.018
^{64}V	518.3	515.5	514.6	-2.89	-3.79	0.000	0.053
^{65}V	520.9	520.1	519.7	-0.80	-1.20	0.108	0.053
^{66}V	524.5	522.5	521.8	-1.98	-2.76	0.184	0.155
^{67}V	527.7	525.9	526.6	-1.79	-1.02	0.220	0.163
^{68}V	529.8	527.5	528.3	-2.33	-1.53	0.233	0.161
^{69}V	531.5	530.9	532.5	-0.70	0.98	0.249	0.169

frame, then the large discrepancy of $\triangle E_2$ with mass number indicate the failure of INM near the drip-line region, or vice versa, (2) similarly if we analyze for $\triangle E_1$, it is somewhat constant with RMF for the entire region considered in the present paper. As we have discussed in the subsection 3, the RMF is based on microscopic origin in mesons and nucleons level. Except few fitted nuclei, all others masses, radii and quadrupole deformation are the predicted results for a large region of the periodic chart. The RMF results are found to be good for almost all the known

Table 4. Same as table 3 for Z = 37 - 40 region.

nucleus	BE(RMF)	BE(FRDM)	BE(INM)	$\triangle E_1$	$\triangle E_2$	β_2 (RMF)	β_2(FRDM)
^{103}Rb	833.0	837.5	836.9	4.50	-0.58	-0.270	0.341
^{104}Rb	836.3	840.0	838.9	3.69	2.53	-0.276	0.333
^{105}Rb	839.4	844.2	842.8	4.78	3.36	-0.284	0.334
^{106}Rb	843.0	846.4	844.5	3.33	1.51	0.000	0.335
^{107}Rb	846.9	849.7	847.5	2.81	0.67	0.000	0.336
^{108}Rb	849.2	851.4	848.2	2.24	-1.00	0.000	0.356
^{109}Rb	851.0	854.0	850.9	3.04	-0.07	0.015	0.373
^{110}Rb	853.3	854.9	851.4	1.54	-1.95	-0.065	0.287
^{111}Rb	855.5	856.4	854.3	0.92	-1.17	-0.08	-0.333
^{112}Rb	857.5	857.0	854.6	-0.47	-2.87	-0.083	-0.340
^{113}Rb	859.6	860.9	857.2	1.23	-2.45	0.097	-0.145
^{114}Rb	861.7	862.1	856.9	0.42	-4.71	0.103	-0.135
^{103}Sr	844.9	850.1	849.4	5.19	4.49	-0.167	0.360
^{104}Sr	848.7	855.1	854.5	6.47	5.88	0.416	0.361
^{105}Sr	852.5	857.8	857.1	5.27	4.60	0.417	0.353
^{106}Sr	856.2	862.6	861.4	6.41	5.26	0.420	0.354
^{107}Sr	860.2	864.8	863.6	4.58	3.44	0.000	0.345
^{108}Sr	864.2	868.8	866.9	4.53	2.71	0.000	0.346
^{109}Sr	867.0	870.4	868.2	3.40	1.26	0.000	0.375
^{110}Sr	869.1	873.5	871.7	4.32	2.54	0.000	0.393
^{111}Sr	871.7	874.6	873.0	2.89	1.36	-0.058	0.393
^{112}Sr	874.2	876.9	876.9	2.80	2.72	-0.073	-0.300
^{113}Sr	876.6	878.9	878.0	2.28	1.45	-0.080	-0.153
^{114}Sr	878.8	882.3	881.0	3.49	2.18	-0.083	-0.153
^{115}Sr	880.9	883.6	882.1	2.69	1.15	-0.082	-0.144
^{116}Sr	882.9	886.5	883.5	3.57	0.51	-0.078	-0.136
^{117}Sr	884.9	887.4	883.0	2.51	-1.90	0.075	-0.128
^{118}Sr	886.8	890.3	879.9	3.45	-6.88	0.059	-0.120
^{119}Sr	888.68	892.6	878.9	3.89	-9.75	0.001	-0.008
^{120}Sr	890.6	895.2	880.4	4.54	-10.28	0.000	0.000
^{105}Y	863.8	868.9	868.9	5.10	5.13	-0.230	0.372
^{106}Y	867.9	872.2	871.9	4.32	4.09	0.419	0.364
^{107}Y	871.9	877.0	876.3	5.11	4.37	0.421	0.364
^{108}Y	876.3	879.9	878.6	3.66	2.31	0.000	0.356
^{109}Y	880.7	884.1	882.6	3.40	1.88	0.000	0.357
^{110}Y	883.8	886.3	884.3	2.46	0.53	0.000	0.386
^{111}Y	886.4	889.6	888.2	3.24	1.86	0.000	0.394
^{112}Y	888.8	890.9	890.1	2.09	1.23	0.000	0.404
^{113}Y	891.4	894.3	893.9	2.91	2.51	-0.047	0.384
^{114}Y	894.1	896.1	895.4	1.97	1.34	-0.071	-0.153
^{115}Y	897.9	899.6	898.7	1.73	0.84	-0.084	-0.153
^{116}Y	899.2	901.7	899.2	2.47	0.03	-0.084	-0.153
^{117}Y	901.5	904.7	900.6	3.15	-0.941	0.064	-0.145
^{107}Zr	882.9	887.9	887.5	5.04	4.60	-0.231	0.364
^{108}Zr	886.9	893.4	892.4	6.50	5.50	0.417	0.365
^{109}Zr	891.6	896.5	895.2	4.87	3.59	0.000	0.357
^{110}Zr	896.3	901.2	899.8	4.93	3.59	0.000	0.368
^{111}Zr	899.8	903.5	901.6	3.70	1.86	0.000	0.387
^{112}Zr	902.7	907.6	906.4	4.83	3.65	0.000	0.395
^{113}Zr	905.5	908.9	908.4	3.37	2.87	0.000	0.404
^{114}Zr	908.5	913.3	912.8	4.79	4.35	-0.167	-0.197
^{115}Zr	911.2	915.4	914.3	4.19	3.03	-0.154	-0.170
^{116}Zr	914.1	919.5	917.8	5.39	3.66	-0.098	-0.162
^{117}Zr	916.9	921.6	918.9	4.72	2.11	-0.097	-0.153
^{118}Zr	919.6	925.3	920.8	5.67	1.12	0.047	-0.153
^{119}Zr	922.5	926.9	920.7	4.49	-1.81	0.001	-0.146

Table 5. Same as table-3 for Z = 60 - 64 region.

nucleus	BE(RMF)	BE(FRDM)	BE(INM)	$\triangle E_1$	$\triangle E_2$	β_2 (RMF)	β_2(FRDM)
^{167}Nd	1310.65	1317.3	1314.9	6.65	4.25	0.31	0.28
^{168}Nd	1313.91	1321.1	1315.3	7.19	1.39	0.3	0.28
^{169}Nd	1317.15	1323.2	1315.5	6.06	-1.64	0.29	0.28
^{170}Nd	1320.27	1326.9	1318.4	6.63	-1.87	0.29	0.27
^{171}Nd	1323.12	1328.9	1319.5	5.79	-3.62	0.28	0.26
^{172}Nd	1325.76	1332.5	1322.5	6.74	-3.26	0.28	0.25
^{173}Nd	1328.16	1334.4	1323.4	6.24	-4.76	0.26	0.24
^{174}Nd	1330.42	1337.8	1325.9	7.38	-4.52	0.25	0.22
^{175}Nd	1333.03	1339.4	1326.6	6.37	-6.43	-0.19	0.21
^{176}Nd	1335.51	1342.6	1328.6	7.09	-6.91	-0.18	0.19
^{177}Nd	1338.14	1343.9	1328.5	5.76	-9.64	-0.13	0.17
^{178}Nd	1341.16	1347	1329.9	5.85	-11.25	-0.12	0.16
^{179}Nd	1344.15	1347.6	1329.5	3.45	-14.65	-0.11	0.18
^{180}Nd	1347.07	1350.6	1330.6	3.53	-16.47	0.09	0.17
^{181}Nd	1350.23	1352	1329.9	1.77	-20.33	0.08	0.15
^{182}Nd	1353.25	1354.9	1331.1	1.65	-22.15	0.07	0.11
^{167}Pm	1321.05	1326.8	1323.1	5.75	2.05	0.33	0.28
^{168}Pm	1324.48	1329.6	1324.3	5.12	-0.18	0.32	0.28
^{169}Pm	1327.84	1333.5	1327.9	5.66	0.06	0.31	0.28
^{170}Pm	1331.15	1336.1	1329.4	4.95	-1.75	0.31	0.28
^{171}Pm	1334.34	1339.8	1332.8	5.46	-1.54	0.3	0.28
^{172}Pm	1337.35	1342.2	1334.3	4.86	-3.05	0.29	0.27
^{173}Pm	1340.15	1345.7	1337.3	5.56	-2.85	0.29	0.26
^{174}Pm	1342.6	1348	1338.5	5.4	-4.1	0.28	0.25
^{175}Pm	1345.01	1351.5	1341.5	6.49	-3.51	-0.2	0.22
^{176}Pm	1347.89	1353.5	1342.4	5.61	-5.49	-0.2	0.21
^{177}Pm	1350.6	1356.7	1344.8	6.1	-5.8	-0.19	0.2
^{178}Pm	1353.15	1358.5	1345.4	5.35	-7.75	-0.18	0.17
^{179}Pm	1355.95	1361.6	1347.3	5.65	-8.65	-0.13	0.16
^{180}Pm	1359	1362.6	1346.9	3.61	-12.09	-0.12	-0.19
^{181}Pm	1362.1	1365.7	1348.5	3.6	-13.6	0.1	-0.18
^{168}Sm	1334.23	1340.5	1337.5	6.27	3.27	0.34	0.28
^{169}Sm	1337.85	1343.3	1339.6	5.45	1.75	0.33	0.28
^{170}Sm	1341.32	1347.8	1343.5	6.48	2.18	0.32	0.28
^{171}Sm	1344.71	1350.4	1345.5	5.69	0.79	0.31	0.28
^{172}Sm	1348.05	1354.6	1349.3	6.55	1.25	0.31	0.28
^{173}Sm	1351.24	1357	1350.8	5.77	-0.43	0.3	0.27
^{174}Sm	1354.19	1361.1	1354.1	6.91	-0.09	0.3	0.26
^{175}Sm	1356.77	1363.4	1355.5	6.63	-1.27	0.29	0.25
^{176}Sm	1359.59	1367.3	1358.5	7.71	-1.09	0.35	0.23
^{177}Sm	1362.3	1369.4	1359.7	7.11	-2.6	-0.2	0.22
^{178}Sm	1365.2	1372.9	1362.3	7.7	-2.9	-0.2	0.2
^{179}Sm	1368	1374.6	1362.9	6.6	-5.1	-0.19	0.17
^{180}Sm	1370.67	1378.1	1365.1	7.43	-5.57	-0.17	0.16
^{181}Sm	1373.66	1379.2	1365.1	5.55	-8.56	-0.13	-0.19
^{182}Sm	1376.79	1382.7	1367.3	5.91	-9.49	-0.12	-0.18
^{183}Sm	1380.03	1384.5	1368.6	4.47	-11.43	0.1	-0.16
^{169}Eu	1346.83	1351.2	1349.6	4.37	2.77	0.34	0.28
^{170}Eu	1350.58	1354.6	1351.8	4.02	1.22	0.34	0.28
^{171}Eu	1354.2	1359.1	1356.4	4.9	2.2	0.33	0.28
^{172}Eu	1357.72	1362.2	1358.8	4.48	1.08	0.32	0.28

continued

continued

nucleus	BE(RMF)	BE(FRDM)	BE(INM)	$\triangle E_1$	$\triangle E_2$	β_2 (RMF)	β_2(FRDM)
^{173}Eu	1361.23	1366.4	1362.9	5.17	1.67	0.31	0.28
^{174}Eu	1364.65	1369.2	1365.1	4.56	0.45	0.31	0.28
^{175}Eu	1367.8	1373.3	1368.6	5.5	0.8	0.31	0.27
^{176}Eu	1370.63	1376	1370.1	5.37	-0.53	0.3	0.26
^{177}Eu	1373.71	1379.9	1373.3	6.2	-0.4	0.35	0.24
^{178}Eu	1376.37	1382.5	1374.7	6.13	-1.67	0.36	0.22
^{179}Eu	1379.41	1385.9	1377.7	6.49	-1.71	-0.2	0.21
^{180}Eu	1382.38	1388.2	1378.9	5.82	-3.48	-0.19	0.18
^{181}Eu	1385.28	1391.6	1381.6	6.32	-3.68	-0.18	0.16
^{182}Eu	1388.14	1393.3	1382.7	5.16	-5.44	-0.16	-0.19
^{183}Eu	1391.32	1396.8	1385.4	5.48	-5.92	-0.13	-0.18
^{171}Gd	1362.7	1367.3	1365.5	4.61	2.81	0.34	0.28
^{172}Gd	1366.46	1372.3	1370.5	5.85	4.05	0.33	0.28
^{173}Gd	1370.19	1375.5	1373.1	5.31	2.91	0.33	0.28
^{174}Gd	1373.93	1380.2	1377.1	6.27	3.17	0.32	0.28
^{175}Gd	1377.53	1383.1	1379.6	5.57	2.07	0.31	0.28
^{176}Gd	1381.02	1387.6	1383.2	6.58	2.18	0.31	0.27
^{177}Gd	1384	1390.3	1385.1	6.3	1.1	0.31	0.26
^{178}Gd	1388.1	1394.6	1388.6	6.5	0.5	0.35	0.24
^{179}Gd	1390.11	1397.2	1390.2	7.09	0.09	0.36	0.22
^{180}Gd	1393.21	1401.1	1393.6	7.89	0.39	-0.2	0.21
^{181}Gd	1396.42	1403.4	1395.5	6.98	-0.92	-0.2	0.19
^{182}Gd	1399.48	1407.1	1398.8	7.62	-0.68	-0.19	0.16
^{183}Gd	1402.46	1408.9	1400.4	6.44	-2.06	-0.17	-0.19
^{184}Gd	1405.6	1412.8	1403.6	7.2	-2	-0.15	-0.18
^{185}Gd	1408.97	1414.9	1404.6	5.93	-4.37	-0.13	-0.16

cases. This prediction not only confine to masses, radii, β_2 but also comes well for other observables. Thus, if we believe all these predictions as success, then the mass formula specially INM needed some modification, specially in the region of Z = 37 - 40 and Z = 60 - 64 which are considered in the current work.

6. Summary and Conclusion

In Summary, we have calculated the binding energy, rms charge and matter radii, quadrupole deformation parameter for the neutron drip-line nuclei having Z = 17 - 23, 37 - 40 and 60 - 64 regions using RMF(NL3*) which are recently predicted to be in *islands of inversion* due to their extra stability compared to the near by isotopes. Since the considered isotopes are experimentally unknown, we compared our results with various mass formula predictions. We found large differences both in binding energy and deformation indicating the special nature of these nuclei. We got some interesting features just like jerk and deep at some places in charge distribution radius which is different from our conventional distribution. In regions Z = 17 - 23, N = 42, Z = 37 - 40, N = 68, and Z= 60 - 64, N = 112 behave as more stable. The true properties of these nuclei can be revealed after the experimental observations.

7. Acknowledgment

The authors thank Institute of Physics, Bhubaneswar, India for hospitality. We thank Prof. S. K. Patra and Prof. L. Satapathy for many stimulating discussions.

References

1. E. K. Warburton, J. A. Becker and B. A. Brown, *Phys. Rev. C* **41** (1990) 1147.
2. E. K. Warburton, J. A. Becker, D. J. Millener and B. A. Brown, *BNL report* 40890 (1987) .
3. E. Caurier, G. Martinez - pinedo, F. Nowacki, A. poves, and A. P. Zuker, *Rev. Mod. Phys.* **77** (2005) 427.
4. S. K. Patra and C. R. Praharaj, *Phys. Letters. B* **273** (1991).
5. J. Duflo and A. Zucker, *Phys. Rev. C* **52** (1996) R23.
6. O. B. Tarasov *et al.*, *Phys. Rev. Lett.* **102** (2009) 142501.
7. S. M. Lenzi *et al.*, *Phys. Rev. C* **82** (2010) 054301 .
8. R. C. Nayak and L. Satapathy, *Atomic and Nuclear Data Tables* **98** (2012) 616.
9. J. D. Walecka, *Ann. Phys. (NY)* **83** (1974) 491.
10. J. Boguta and A. R. Bodmer, *Nucl. Phys. A* **292** (1977) 413.
11. B. D. Serot and J. D. Walecka, *Adv. Nucl. Phys.* **16** (1986) 1.
12. C. J. Horowitz and B. D. Serot, *Nucl. Phys. A* **368** (1981) 503.
13. C. E. Price and G. E. Walker, *Phys. Rev. C* **36** (1987) 354.
14. B. D. Serot and J. D. Walecka, *Int. J. Mod. Phys. E* **6** (1997) 515.
15. D. Vretenar, A. V. Afanasjev, G. A. Lalazissis, P.Ring,*Phys.Rep.* **409** (2005) 101.
16. T. Niksic et al., *Prog. Part. Nucl. Phys.* **66** (2011) 519.
17. Y. K. Gambhir, P. Ring and A. Thimet, *Ann. Phys. (NY)* **198** (1990) 132.
18. G. A. Lalazissis, S. Karatzikos, R. Fossion, D. Pena Arteaga, A. V. Afanasjev and P. Ring, *Phys. Lett. B* **671** (2009) 36.
19. S. K. Patra and C. R. Praharaj, *Phys. Rev. C* **44** (1991) 2552.
20. S. K. Patra, *Phys. Rev. C* **48**, 1449 (1993).
21. Y. K. Gambhir, P. Ring, and A. Thimet, *Ann. Phys. (N.Y.)* **198**, 132 (1990).
22. M. A. Preston and R. K. Bhaduri, *Structure of Nucleus, Addison-Wesley Publishing Company, 1982*, Ch. 8, page 309.
23. D. G. Madland and J. R. Nix, *Nucl. Phys. A* **476**, 1 (1981).
24. P. Möller and J.R. Nix, *At. Data and Nucl. Data Tables* **39**, 213 (1988).
25. J. Dobaczewski, H. Flocard and J. Treiner, *Nucl. Phys. A* **422**, 103 (1984).
26. J. Dobaczewski, W. Nazarewicz, T.R. Werner, J.F. Berger, C.R. Chinn and J. Decharge, *Phys. Rev. C* **53**, 2809 (1996).
27. S. K. Patra, M. Del Etal, M. Centelles, and X. Vinas, *Phy. Rev. C* **63**, 024311 (2001).
28. T. R. Werner, J. A. Sheikh, W. Nazarewicz, M. R. Strayer, A. S. Umar, and M. Mish, *Phys. Lett. B* **335**, 259 (1994).
29. T. R. Werner, J. A. Sheikh, M. Mish, W. Nazarewicz, J. Rikovska, K. Heeger, A. S. Umar, and M. R. Strayer, *Nucl. Phys. A* **597**, 327 (1996).
30. G. A. Lalazissis, D. Vretener, P. Ring, M. Stoitsor and L. M. Robledo, *Phys. Rev. C* **60**, 014310 (1999).
31. G. A. Lalazissis, D. Vretenar, and P. Ring, *Nucl. Phys. A* **650**, 133 (1999).
32. P. Arumugam, B. K. Sharma, S. K. Patra and Raj Kumar Gupta, *Phys. Rev. C* **71**, 064308 (2005).
33. S. K. Patra, P. Arumugam and L. Satpathy, Bulletin Board nucl-th/0504063.
34. P. Möller, J. R. Nix, W. D. Myers and W. J. Swiatecki, *Atomic and Nucl. Data Tables* **59** (1995) 185.

35. P. Möller, J. R. Nix and K. -L. Kratz, *Atomic and Nucl. Data Tables* **66** (1997) 131.
36. K. Tshoo et al., *Phys. Rev. Lett.* **109**, (2012) 022501.